Available online at www.sciencedirect.com
SCIENCE DIRECT®
Journal of Sound and Vibration 282 (2005) 991–1007
JOURNAL OF SOUND AND VIBRATION
www.elsevier.com/locate/jsvi

Forced vibrations of solid elastic cylinders

D.D. Ebenezer[a,*], K. Ravichandran[a], Chandramouli Padmanabhan[b]

[a]*Naval Physical and Oceanographic Laboratory, Thrikkakara, Kochi 682 021, India*
[b]*Department of Applied Mechanics, Indian Institute of Technology—Madras, Chennai 600 036, India*

Received 25 November 2003; received in revised form 15 March 2004; accepted 17 March 2004
Available online 28 October 2004

Abstract

A method is presented to determine the vibration response of a solid, elastic, isotropic cylinder with arbitrary length to radius ratio when subject to arbitrary distribution of axisymmetric excitation on its surfaces. In this method, the axial and radial components of displacement are expressed as a sum of two infinite series. Each term in both the series is an exact solution to the governing equations of motion and has a coefficient that is used to satisfy boundary conditions. One series contains Bessel functions that form a complete set in the radial direction and the other contains trigonometric functions that form a complete set in the axial direction. The components of stress are also expressed in terms of complete sets of functions by using the expression for displacement. The coefficients in the series are determined by using the orthogonal properties of the functions to satisfy the boundary conditions in a mean-square-error sense. Numerical results are presented to illustrate the broadband responses of cylinders to uniform and concentrated loads on the flat and curved surfaces. They are in good agreement with results obtained using ATILA—a commercial finite-element software.

1. Introduction

Soldatos [1] presented a detailed review of three-dimensional dynamic analyses of infinite and finite circular cylinders and cylindrical shells in 1994. The review includes several methods used to study circular cylinders of finite length. Hutchinson used infinite series to determine the resonance

*Corresponding author. Fax: +91-484-2424858.
E-mail address: tsonpol@vsnl.com (D.D. Ebenezer).

0022-460X/$ - see front matter © 2004 Elsevier Ltd. All rights reserved.
doi:10.1016/j.jsv.2004.03.070

frequencies and eigenmodes of isotropic cylinders. He investigated solid cylinders encased in a rigid container [2], axisymmetric vibrations of free solid cylinders [3], and three-dimensional vibrations of free solid [4] and hollow cylinders [5]. Lusher and Hardy [6] used the same method to analyze transversely isotropic cylinders. Rumermann and Raynor [7] found the axisymmetric resonance frequencies and eigenmodes of solid isotropic cylinders with free lateral surface and free ends and fixed lateral surface and free ends. They expressed the components of displacement as weighted sums of the corresponding pure radial and axial modes of the infinite cylinder and used the Ritz method. Gladwell et al. [8] used the finite element method. McMahon [9] used the finite difference method to study the free vibrations of axisymmetric solid isotropic cylinders. Heyliger [10] and Soldatos and Hadjigeorgiou [11] used power series and fictitious layers in conjunction with the Ritz method and the governing differential equations, respectively, to analyze the free vibration of anisotropic cylinders.

After 1994, there have been more investigations of the resonance frequencies and mode shapes of finite cylinders. Leissa and So [12,13] presented tables of resonance frequencies of solid, elastic, free–free and free–fixed cylinders with various length to radius ratios and Poisson's ratios using the Ritz method. Their results are in excellent agreement with Hutchinson's results [14,15]. Buchanan and Chua [16] used the finite element method to study isotropic and anisotropic cylinders with free–fixed and fixed–fixed flat surfaces. Kari [17,18] presented the resonance frequencies and mode shapes of cylinders with stress-free curved surface and free, clamped, simply supported, and slip conditions on the flat surfaces. Zhou et al. [19] used the Chebyshev–Ritz method to determine the lower and higher order resonance frequencies of solid and hollow cylinders that are completely free or fixed on one of the flat surfaces.

Earlier, Holland and Eer Nisse [20] used a Ritz approach to determine the resonance frequencies and eigenmodes of free–free transversely isotropic solid cylinders. They used complete sets of frequency-independent trial functions that did not satisfy the governing equations or the boundary conditions. They obtained faster convergence by using over-complete sets.

Chau and Wei [21] analyzed solid isotropic cylinders subjected to arbitrary static loads using infinite series. They determined the response of the cylinder to a patch load [22].

Several investigations over the last half-century, including the one presented here, of the vibration of elastic cylinders are motivated by a desire to understand and model piezoelectric transducers. However, the forced vibration of a finite cylinder is of interest in all fields.

In this paper, the method used by Hutchinson to study the free vibrations of cylinders is extended to determine the vibration response of solid, elastic, isotropic, cylinders to arbitrary distributions of certain functions on the boundaries. Each component of displacement in the cylinder is expressed as the sum of two infinite series. Each term in both the series is an exact solution to the governing equations of motion and has a coefficient that is used to satisfy boundary conditions. One series contains Bessel functions that form a complete set in the radial direction and the other contains trigonometric functions that form a complete set in the axial direction. The stress components are also expressed in terms of complete sets of functions by using the expressions for displacement. The coefficients in the series are determined by using the orthogonal properties of the function to satisfy the boundary conditions in a mean-square-error sense. Numerical results are presented to illustrate the broadband response of the cylinder to uniform and concentrated loads on the flat and curved surfaces. They are in good agreement with results obtained using ATILA [23]—a commercial finite-element software.

2. Theoretical analysis

Consider a solid, elastic, isotropic cylinder of finite length L and radius a as shown in Fig. 1. Non-uniform, axisymmetric, stresses or displacements are specified on the surfaces of the cylinder. The response of the cylinder is of interest. The response to non-axisymmetric excitations can be determined by using Fourier series expansions in the tangential direction.

The excitation and, therefore, the response of the cylinder are axisymmetric. The dynamic equilibrium equations are expressed in cylindrical coordinates (r, θ, z) as

$$\frac{\partial T_{zz}}{\partial z}+\frac{\partial T_{rz}}{\partial r}+\frac{1}{r}T_{rz}=-\rho\omega^2 U \tag{1a}$$

and

$$\frac{\partial T_{rr}}{\partial r}+\frac{\partial T_{rz}}{\partial z}+\frac{1}{r}(T_{rr}-T_{\theta\theta})=-\rho\omega^2 W, \tag{1b}$$

where U and W are the axial and radial displacements, respectively, T_{rr}, T_{zz} and $T_{\theta\theta}$ are normal components of stress, T_{rz} is a shear component of stress, ρ is the density and ω is the angular frequency. The components of strain are

$$\left[S_{rr},\quad S_{\theta\theta},\quad S_{zz},\quad S_{rz}\right]=\left[\frac{\partial W}{\partial r},\quad \frac{W}{r},\quad \frac{\partial U}{\partial z},\quad \frac{\partial U}{\partial r}+\frac{\partial W}{\partial z}\right]. \tag{2}$$

The constitutive relations for an isotropic elastic cylinder are

$$\begin{Bmatrix} T_{rr}\\ T_{\theta\theta}\\ T_{zz}\\ T_{rz}\end{Bmatrix}=\begin{bmatrix} \lambda+2\mu & \lambda & \lambda & 0\\ \lambda & \lambda+2\mu & \lambda & 0\\ \lambda & \lambda & \lambda+2\mu & 0\\ 0 & 0 & 0 & \mu\end{bmatrix}\begin{Bmatrix} S_{rr}\\ S_{\theta\theta}\\ S_{zz}\\ S_{rz}\end{Bmatrix}, \tag{3}$$

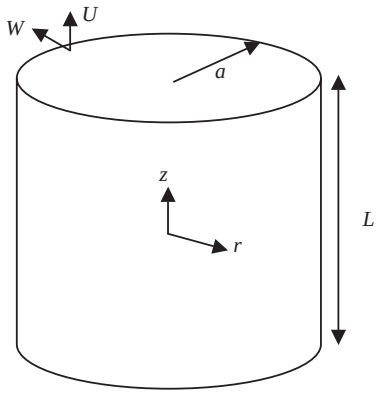

Fig. 1. A solid cylinder of length L and radius a. The axial and radial components of displacement are U and W, respectively.

where λ and μ are the Lamé's constants. The exact axisymmetric governing equations are obtained by substituting Eqs. (2) and (3) in Eq. (1) and expressed as

$$\begin{bmatrix} (\lambda+2\mu)\dfrac{\partial^2}{\partial z^2}+\mu\left[\dfrac{\partial^2}{\partial r^2}+\dfrac{1}{r}\dfrac{\partial}{\partial r}\right]+\rho\omega^2 & (\lambda+\mu)\left[\dfrac{\partial^2}{\partial r\,\partial z}+\dfrac{1}{r}\dfrac{\partial}{\partial z}\right] \\ (\lambda+\mu)\dfrac{\partial^2}{\partial r\,\partial z} & (\lambda+2\mu)\left[\dfrac{\partial^2}{\partial r^2}+\dfrac{1}{r}\dfrac{\partial}{\partial r}-\dfrac{1}{r^2}\right]+\mu\dfrac{\partial^2}{\partial z^2}+\rho\omega^2 \end{bmatrix}\begin{Bmatrix} U \\ W \end{Bmatrix}=\begin{Bmatrix} 0 \\ 0 \end{Bmatrix}. \tag{4}$$

It is easily verified that [3,24]

$$\begin{bmatrix} U & W \end{bmatrix}^{\mathrm{T}}=\begin{bmatrix} U_1 & W_1 \end{bmatrix}^{\mathrm{T}}+\begin{bmatrix} U_2 & W_2 \end{bmatrix}^{\mathrm{T}} \tag{5a}$$

is the sum of two exact solutions to Eq. (4) where

$$\begin{Bmatrix} U_1 \\ W_1 \end{Bmatrix}=\begin{Bmatrix} A\sin(Kz) \\ 0 \end{Bmatrix}+\begin{Bmatrix} \sum_{m=1}^{M_r}\sum_{s=1}^{2} A_{ms}\mathrm{J}_0(k_{rm}r)\,\sin(k_{zms}z) \\ \sum_{m=1}^{M_r}\sum_{s=1}^{2} A_{ms}\psi_{ms}\mathrm{J}_1(k_{rm}r)\,\cos(k_{zms}z) \end{Bmatrix}, \tag{5b}$$

$$\begin{Bmatrix} U_2 \\ W_2 \end{Bmatrix}=\begin{Bmatrix} 0 \\ B\mathrm{J}_1(Kr) \end{Bmatrix}+\begin{Bmatrix} \sum_{m=1}^{M_z}\sum_{s=1}^{2} B_{ms}\mathrm{J}_0(k_{rms}r)\,\sin(k_{zm}z) \\ \sum_{m=1}^{M_z}\sum_{s=1}^{2} B_{ms}\chi_{ms}\mathrm{J}_1(k_{rms}r)\,\cos(k_{zm}z) \end{Bmatrix}, \tag{5c}$$

$$K=\omega\sqrt{\frac{\rho}{(\lambda+2\mu)}}, \tag{5d}$$

and J_μ is the μth order Bessel function of the first kind. Eqs. (5b) and (5c) are exact solutions for arbitrary values of k_{rm}, $m=1, 2, 3,\ldots,M_r$ and k_{zm}, $m=1, 2, 3,\ldots,M_z$.

The frequency-dependent values of k_{zms} are determined by substituting Eq. (5b) into Eq. (4) and equating the determinant of the resulting equation to zero. The characteristic equation is quadratic in k_{zms}^2 and is solved for $m=1, 2,\ldots,M_r$ to obtain

$$k_{zm1}=\sqrt{\frac{\rho\omega^2}{\mu}-k_{rm}^2} \tag{6a}$$

and

$$k_{zm2}=\sqrt{\frac{\rho\omega^2}{(\lambda+2\mu)}-k_{rm}^2}. \tag{6b}$$

Similarly, the frequency-dependent values of k_{rms} are determined by substituting Eq. (5c) in Eq. (4) and equating the determinant of the resulting equation to zero. The characteristic equation is quadratic in k_{rms}^2 and is solved for $m=1, 2,\ldots,M_z$ obtain

$$k_{rm1}=\sqrt{\frac{\rho\omega^2}{\mu}-k_{zm}^2} \tag{7a}$$

and

$$k_{rm2} = \sqrt{\frac{\rho\omega^2}{(\lambda+2\mu)} - k_{zm}^2}. \tag{7b}$$

ψ_{ms} and χ_{ms} are then obtained by substituting Eqs. (5b) and (5c), respectively, in Eq. (4) and rearranging. They are expressed as

$$\psi_{ms} = \frac{(\lambda+\mu)k_{zms}k_{rm}}{\left[\rho\omega^2 - (\lambda+2\mu)k_{rm}^2 - \mu k_{zms}^2\right]} \tag{8a}$$

and

$$\chi_{ms} = \frac{(\lambda+\mu)k_{zm}k_{rms}}{\left[\rho\omega^2 - (\lambda+2\mu)k_{rms}^2 - \mu k_{zm}^2\right]}, \tag{8b}$$

respectively.

In this paper, $k_{rm}a$ are chosen to be the roots of $\mathrm{J}_1(k_{rm}a) = 0$ and are approximately equal to 0, 3.83, 7.02, 10.17,… for $m = 0, 1, 2, 3,\ldots$ respectively. In the leading term in Eq. (5b) that corresponds to $m = 0$, $k_{rm}a$ and radial displacement are zero but axial displacement is non-zero and a function of Kz. Similarly, $k_{zm}L/2$ are chosen to be $m\pi$ with $m = 0, 1, 2, 3\ldots$ In the leading term in Eq. (5c) that corresponds to $m = 0$, the axial displacement is zero and the radial displacement is a function of Kr.

The values of $k_{rm}a$ and $k_{zm}L/2$ are chosen such that the displacements on the flat and curved surfaces are expressed in terms of complete sets of functions. It is noted that for $M_r = \infty$, $\mathrm{J}_\mu(k_{rm}r)$ form a point-wise complete set of functions when $\mu = 0$ and a norm-wise complete set of functions when $\mu = 1$, i.e.,

$$\int_0^a \mathrm{J}_\mu(k_{rm}r)\mathrm{J}_\mu(k_{rn}r)r\,\mathrm{d}r = \begin{cases} 0 & m \neq n, \\ \frac{a^2}{2}\mathrm{J}_0^2(k_{rm}a) & m = n, \end{cases} \quad \mu = 0 \text{ or } 1, \ m = 0, 1, 2, \ldots . \tag{9}$$

(Sets of functions that are not all zero at the same point and form a norm-wise complete set of functions are known as point-wise complete sets.) Similarly, for $M_z = \infty$, $\sin(k_{zm}z)$ and $\cos(k_{zm}z)$ form norm-wise and point-wise complete sets of functions, respectively, i.e.,

$$\int_{-L/2}^{+L/2} \sin(k_{zm}z)\sin(k_{zn}z)\,\mathrm{d}z = \begin{cases} 0, & m \neq n, \\ L/2, & m = n \end{cases} \tag{10a}$$

and

$$\int_{-L/2}^{+L/2} \cos(k_{zm}z)\cos(k_{zn}z)\,\mathrm{d}z = \begin{cases} 0, & m \neq n, \\ L/2, & m = n. \end{cases} \tag{10b}$$

The axial displacement in Eq. (5) is antisymmetric about the centre of the cylinder. A symmetric axial displacement can be obtained by using *sin* in place of *cos* and *cos* in place of *sin*. The Bessel function of the second kind has not been included in Eqs. (5b) and (5c) to satisfy the finiteness condition at the origin. If the cylinder is hollow, this function should also be included.

Other quantities of interest are now easily determined by using Eqs. (2),(3),and (5). The normal components of stress are expressed as

$$T_{rr} = A[K\lambda\cos(Kz)] + B\left[(\lambda+2\mu)K\mathrm{J}_0(Kr) - \frac{2\mu}{r}\mathrm{J}_1(Kr)\right] + \sum_{m=1}^{M_r}\sum_{s=1}^{2} A_{ms}\left\{[\lambda k_{zms} + (\lambda+2\mu)\psi_{ms}k_{rm}]\mathrm{J}_0(k_{rm}r) - \frac{2\mu}{r}\psi_{ms}\mathrm{J}_1(k_{rm}r)\right\}\cos(k_{zms}z) + \sum_{m=1}^{M_z}\sum_{s=1}^{2} B_{ms}\left\{[\lambda k_{zm} + (\lambda+2\mu)\chi_{ms}k_{rms}]\mathrm{J}_0(k_{rms}r) - \frac{2\mu}{r}\chi_{ms}\mathrm{J}_1(k_{rms}r)\right\}\cos(k_{zm}z) \quad (11)$$

and

$$T_{zz} = A[(\lambda+2\mu)K\cos(Kz)] + B[\lambda K\mathrm{J}_0(Kr)] + \sum_{m=1}^{M_r}\sum_{s=1}^{2} A_{ms}\mathrm{J}_0(k_{rm}r)[(\lambda+2\mu)k_{zms} + \lambda\psi_{ms}k_{rm}]\cos(k_{zms}z) + \sum_{m=1}^{M_z}\sum_{s=1}^{2} B_{ms}\mathrm{J}_0(k_{rms}r)[(\lambda+2\mu)k_{zm} + \lambda\chi_{ms}k_{rms}]\cos(k_{zm}z). \quad (12)$$

The shear stress is expressed as the sum of two series:

$$T_{rz} = -\mu\sum_{m=1}^{M_r}\sum_{s=1}^{2} A_{ms}\mathrm{J}_1(k_{rm}r)[k_{rm} + \psi_{ms}k_{zms}]\sin(k_{zms}z) - \mu\sum_{m=1}^{M_z}\sum_{s=1}^{2} B_{ms}\mathrm{J}_1(k_{rms}r)[k_{rms} + \chi_{ms}k_{zm}]\sin(k_{zm}z). \quad (13)$$

It is noted that each term in the first series is zero at $r=a$ and each term in the second series is zero at $z=\pm L/2$.

All the components of displacement and stress are expressed in terms of over-complete sets of functions in both the axial and radial directions. (An over-complete set of functions is the sum a point-wise or norm-wise complete set of functions and other functions.) In the radial direction, $\mathrm{J}_0(k_{rm}r)$, $m=0,1,2,\ldots,\infty$ form a point-wise complete set of functions: U, T_{rr} and T_{zz} are expressed as a weighted sum of these functions and other terms. Further, $\mathrm{J}_1(k_{rm}r)$, $m=1,2,\ldots,\infty$ are all zero at $r=0$ and a, and form a norm-wise complete set of functions: W and T_{rz} are expressed as a weighted sum of these functions and other terms. Similarly, in the axial direction, $\cos(k_{zm}z)$, $m=0,1,2,\ldots,\infty$ and $\sin(k_{zm}z)$, $m=1,2,\ldots,\infty$ form point-wise and norm-wise complete sets of functions: the components of displacement and stress are expressed as the sum of either one of these sets of functions and other terms. In brief, the components of displacement and stress are expressed in terms of complete sets of functions. It, therefore, follows that arbitrary distributions of displacement and stress can be expressed in terms of these functions and the response of the cylinder can be determined for arbitrary excitations.

3. Special cases

Several special cases are presented to illustrate the procedure for finding the response of the cylinder to non-uniform, axisymmetric excitations. The stress on the surface of the cylinder is specified in all the cases. However, a similar procedure can be used when the displacements are specified.

Let the normal and shear stress on the flat surfaces be denoted by $\bar{T}_{zz}$ and $\bar{T}_{rz}$, respectively, and the normal and shear stress on the curved surface be denoted by $\widehat{T}_{rr}$ and $\widehat{T}_{rz}$, respectively, i.e.,

$$T_{zz} = \bar{T}_{zz} \text{ and } T_{rz} = \bar{T}_{rz} \text{ on } 0 \leqslant r \leqslant a,\ z = \pm L/2, \tag{14a,14b}$$

and

$$T_{rr} = \widehat{T}_{rr} \text{ and } T_{rz} = \widehat{T}_{rz} \text{ on } r = a,\ |z| \leqslant L/2. \tag{14c,14d}$$

The boundary condition on T_{zz} in Eq. (14a) is satisfied by using the orthogonal property of $\mathrm{J}_0(k_{rn}a)$. Substituting Eq. (14a) in Eq. (12), multiplying both sides by $r\mathrm{J}_0(k_{rn}r)$ and integrating over r, yields

$$A\left[(\lambda+2\mu)\frac{Ka^2}{2}\cos\left(\frac{KL}{2}\right)\right] + B[\lambda a \mathrm{J}_1(Ka)] + \sum_{m=1}^{M_z}\sum_{s=1}^{2} B_{ms}(-1)^m[(\lambda+2\mu)k_{zm} + \lambda\chi_{ms}k_{rms}]\frac{a}{k_{rms}}J_1(k_{rms}a) = \int_0^a \bar{T}_{zz} r\,\mathrm{d}r, \quad n = 0 \tag{15a}$$

and

$$B[\lambda K R(K)] + \sum_{s=1}^{2} A_{ns}\cos\left(\frac{k_{zns}L}{2}\right)\left[(\lambda+2\mu)k_{zns} + \lambda\psi_{ns}k_{rn}\right]R(k_{rn}) + \sum_{m=1}^{M_z}\sum_{s=1}^{2} B_{ms}(-1)^m\left[(\lambda+2\mu)k_{zm} + \lambda\chi_{ms}k_{rms}\right]R(k_{rms}) = \int_0^a \bar{T}_{zz}\mathrm{J}_0(k_{rn}r) r\,\mathrm{d}r, \quad n = 1, 2, \ldots \tag{15b}$$

by using [25]

$$\int_0^a \mathrm{J}_0(Xr)\mathrm{J}_0(k_{rn}r) r\,\mathrm{d}r = R(X), \tag{16a}$$

where

$$R(X) = \begin{cases} 0, & X = k_{rm},\ m \neq n, \\ \frac{a^2}{2}\mathrm{J}_0^2(k_{rn}a) & X = k_{rn},\ m = n, \\ \frac{Xa}{X^2 - k_{rn}^2}\mathrm{J}_0(k_{rn}a)\mathrm{J}_1(Xa) & X \neq k_{rn},\ n = 1, 2, 3, \ldots\ . \end{cases} \tag{16b}$$

The boundary condition on T_{rz} in Eq. (14b) is satisfied by substituting it in Eq. (13), and using the orthogonal property of $\mathrm{J}_1(k_{rn}r)$ in Eq. (9). Multiplying both sides of Eq. (13) by $r\mathrm{J}_1(k_{rn}r)$ and

integrating over r yields

$$-\mu\frac{a^2}{2}\mathrm{J}_0^2(k_{rn}a)\sum_{s=1}^{2}A_{ns}[k_{rn}+\psi_{ns}k_{zns}]\sin\left(k_{zns}L/2\right)=\int_0^a \bar{T}_{rz}\mathrm{J}_1(k_{rn}r)r\,\mathrm{d}r,\quad n=1.2.\ldots\ . \tag{17}$$

The boundary condition on T_{rr} in Eq. (14c) is satisfied by substituting it into Eq. (11) and using the orthogonal property of $\cos(k_{zm}z)$ in Eq. (10). Multiplying both sides of Eq. (11) by $\cos(k_{zn}z)$ and integrating over z yields

$$A\left[2\lambda\sin\left(\frac{KL}{2}\right)\right]+B\left[(\lambda+2\mu)K\mathrm{J}_0(Ka)-\frac{2\mu}{a}\mathrm{J}_1(Ka)\right]L$$
$$+\sum_{m=1}^{M_r}\sum_{s=1}^{2}A_{ms}2\left[\lambda+\frac{(\lambda+2\mu)}{k_{zms}}\psi_{ms}k_{rm}\right]\mathrm{J}_0(k_{rm}a)\sin\left(\frac{k_{zms}L}{2}\right)=\int_{-L/2}^{L/2}\widehat{T}_{rr}\,\mathrm{d}z,\quad n=0, \tag{18a}$$

and

$$A[K\lambda S(K)]+\sum_{m=1}^{M_r}\sum_{s=1}^{2}A_{ms}[\lambda k_{zms}+(\lambda+2\mu)\psi_{ms}k_{rm}]\mathrm{J}_0(k_{rm}a)S(k_{zms})$$
$$+\sum_{s=1}^{2}B_{ns}\left\{[\lambda k_{zn}+(\lambda+2\mu)\chi_{ns}k_{rns}]\mathrm{J}_0(k_{rns}a)-\frac{2\mu}{a}\chi_{ns}\mathrm{J}_1(k_{rns}a)\right\}S(k_{zn})$$
$$=\int_{-L/2}^{L/2}\widehat{T}_{rr}\cos(k_{zn}z)\,\mathrm{d}z,\quad n=1,2,\ldots\ . \tag{18b}$$

by using

$$\int_{-L/2}^{+L/2}\cos(Xz)\cos(k_{zn}z)\,\mathrm{d}z=S(X), \tag{19a}$$

where

$$S(X)=\begin{cases}0, & X=k_{zm}\ \ m\neq n\\ L/2, & X=k_{zn}\ \ m=n\\ \frac{2(-1)^{n+1}XL^2}{(4n^2\pi^2-X^2L^2)}\sin\left(\frac{XL}{2}\right), & X\neq k_{zn}\ \ n=1,2,3,\ldots\ .\end{cases} \tag{19b}$$

The boundary condition on T_{rz} in Eq. (14d) is satisfied by substituting it into Eq. (13) and using the orthogonal property of $\sin(k_{zm}z)$ in Eq. (10). Multiplying both sides of Eq. (13) by $\sin(k_{zn}z)$ and integrating over z yields

$$-\mu\frac{L}{2}\sum_{s=1}^{2}B_{ns}\left[k_{rns}+\chi_{ns}k_{zn}\right]\mathrm{J}_1(k_{rns}a)=\int_{-L/2}^{L/2}\widehat{T}_{rz}\sin(k_{zn}z)\,\mathrm{d}z,\ \ n=1,2,\ldots\ . \tag{20}$$

Eqs. (15)–(20) are combined, truncated, and expressed in matrix form as

$$[\mathbf{F}]\{\mathbf{X}\}=\{\mathbf{G}\}, \tag{21a}$$

where

$$\{\mathbf{X}\}^{\mathrm{T}} = \left[A, B, A_{11}, A_{12}, A_{21}, A_{22}, \ldots, A_{M_r 1}, A_{M_r 2}, B_{11}, B_{12}, B_{21}, B_{22}, \ldots, B_{M_z 1}, B_{M_z 2}\right], \tag{21b}$$

[**F**] is a square matrix of size $[2(M_r + M_z + 1),\ 2(M_r + M_z + 1)]$, and M_r and M_z are now finite. The elements of the column matrix **G** are zero when there is no stress on the boundaries. Hutchinson [3], in essence, condensed [**F**] to a matrix of smaller size by rearranging the equations before computing the resonance frequencies.

3.1. Case 1A

The stress on the surfaces, except $\bar{T}_{zz}$ inside a circle of radius a/N, is zero everywhere, i.e.,

$$\bar{T}_{zz} = \begin{cases} -1 & \text{on } 0 \leqslant r \leqslant a/N,\ z = \pm L/2 \\ 0 & \text{on } a/N < r \leqslant a,\ z = \pm L/2 \end{cases}, \tag{22a}$$

$$\bar{T}_{rz} = 0, \quad \widehat{T}_{rz} = 0, \tag{22b,22c}$$

and

$$\widehat{T}_{rr} = 0. \tag{22d}$$

It therefore follows that the non-zero elements of {**G**} are

$$G_1 = \int_0^a \bar{T}_{zz} r \, \mathrm{d}r = -\frac{a^2}{2N^2}, \tag{23a}$$

$$G_{n+1} = \int_0^a \bar{T}_{zz} \mathrm{J}_0(k_{rn} r) r \, \mathrm{d}r = -\frac{a}{N k_{rn}} \left[\mathrm{J}_1\left(\frac{k_{rn} a}{N}\right)\right], \quad n = 1, 2, \ldots, M_r. \tag{23b}$$

3.2. Case 1B

The stress on the surfaces, except $\bar{T}_{zz}$ outside a circle of radius a/N, is zero everywhere, i.e., the boundary conditions are

$$\bar{T}_{zz} = \begin{cases} 0 & \text{on } 0 \leqslant r < a/N,\ z = \pm L/2 \\ -1 & \text{on } a/N \leqslant r \leqslant a,\ z = \pm L/2 \end{cases} \tag{24}$$

and Eqs. (22b),(22c) and (22d).

It therefore follows that the non-zero elements of **G** are

$$G_1 = \int_0^a \bar{T}_{zz} r \, \mathrm{d}r = -\frac{a^2\left(N^2 - 1\right)}{2N^2}, \tag{25a}$$

$$G_{n+1} = \int_0^a \bar{T}_{zz} \mathrm{J}_0(k_{rn} r) r \, \mathrm{d}r = \frac{a}{N k_{rn}} \mathrm{J}_1\left(\frac{k_{rn} a}{N}\right), \quad n = 1, 2, \ldots, M_r. \tag{25b}$$

3.3. Case 2A

The stresses on the surfaces, except $\widehat{T}_{rr}$ inside a band, are zero everywhere, i.e., the boundary conditions are

$$\bar{T}_{zz} = 0 \quad \text{on } 0 \leqslant r \leqslant a,\ z = \pm L/2, \tag{26a}$$

Eqs. (22b) and (22c), and

$$\widehat{T}_{rr} = \begin{cases} -1 & \text{on } r = a, \quad |z| \leqslant L/N, \\ 0 & \text{on } r = a, \quad L/N < |z| \leqslant L/2. \end{cases} \tag{26b}$$

The only non-zero elements of **G** are

$$G_{2M_r+2} = \int_{-L/N}^{L/N} \widehat{T}_{rr}\,\mathrm{d}z = -\frac{2L}{N}, \tag{27a}$$

$$G_{2M_r+n+2} = \int_{-L/N}^{L/N} \widehat{T}_{rr}\cos(k_{zn}z)\,\mathrm{d}z = -\frac{L}{n\pi}\sin\left(\frac{2n\pi}{N}\right),\ n = 1, 2, \ldots, M_z. \tag{27b}$$

3.4. Case 2B

The stress on the surfaces, except $\widehat{T}_{rr}$ inside two bands, is zero everywhere, i.e., the boundary conditions are Eqs. (26a),(22b) and (22c) and

$$\widehat{T}_{rr} = \begin{cases} 0 & \text{on } r = a, \quad |z| < L/N, \\ -1 & \text{on } r = a, \quad L/N \leqslant |z| \leqslant L/2. \end{cases} \tag{28}$$

The only non-zero elements of **G** are

$$G_{2M_r+2} = \int_{-L/N}^{L/N} \widehat{T}_{rr}\,\mathrm{d}z = -\frac{L(N-2)}{N}, \tag{29a}$$

$$G_{2M_r+n+2} = \int_{-L/N}^{L/N} \widehat{T}_{rr}\cos(k_{zn}z)\,\mathrm{d}z = \frac{L}{n\pi}\sin\left(\frac{2n\pi}{N}\right),\ n = 1, 2, \ldots, M_z. \tag{29b}$$

4. Numerical results and discussion

Numerical results are presented for a solid elastic cylinder to illustrate free and forced responses. The Young modulus, Y, the Poisson ratio, σ, and density, of the cylinder are 200 GPa, 0.3, and 7800 kg/m^3 respectively, i.e., the Lame's constants are $\lambda \approx 115.38$ GPa and $\mu \approx 76.923$ GPa, respectively. The diameter and length of the cylinder are 10 mm each. Solid lines and dots are used to show forced responses obtained using the present approach and ATILA, respectively. In the present approach $M_r = M_z = 20$ is used to obtain the forced responses shown

Table 1
Resonance frequencies of a cylinder (Young's modulus = 200 GPa, the Poisson ratio 0.3, density 7800 kg/m^3) of length and diameter 10 mm each computed using various methods

Mode no.	Resonance frequency (kHz)					
	Leissa and So [13]	ATILA [23]	Present method			
			$M_r = M_z = 5$	$M_r = M_z = 10$	$M_r = M_z = 20$	$M_r = M_z = 200$
1	232.5	232.5	232.7	232.6	232.5	232.5
2	306.6	306.6	307.2	306.8	306.6	306.6
3	398.7	398.8	398.8	398.8	398.7	398.8
4	489.4	489.4	489.7	489.5	489.6	489.5
5	559.1	559.0	561.6	559.8	559.2	559.0
6		686.7	687.4	686.9	686.8	686.7
7		708.0	708.2	708.2	708.0	708.0
8		830.5	834.8	831.8	830.8	830.8
9		862.3	863.2	862.5	862.3	862.3
10		903.5	903.7	903.5	903.5	903.5
11		942.5	941.4	943.0	942.6	942.5
12		990.2	990.6	990.3	990.1	990.2

in the figures. In ATILA, 8 noded, axisymmetric, rectangular, quadratic elements are used to model half the cylinder. All forced responses are computed only at frequencies that are integer multiples of 10 kHz.

The resonance frequencies of the completely free cylinder that are less than 1 MHz, obtained by using finite values of M_r and M_z, are shown in Table 1. For values of $M_r = M_z$ less than or equal to 12 the resonance frequencies are obtained by finding the minima in the determinant of [**F**] For higher values of M_r and M_z [**F**] is ill-conditioned and the resonance frequencies are obtained by finding the frequencies at which the smallest eigenvalue of [**F**] reaches a local minimum, i.e., through singular value decomposition. Resonance frequencies obtained using Leissa and So [13] and ATILA [23] are also shown in Table 1. In ATILA, 1600 square elements are used. It is seen that there is good agreement between the three methods.

The difference in the resonance frequencies obtained using the present method and ATILA is less than 0.1%, except for the resonances approximately at 307, 560, and 830 kHz even when M_r and M_z are only 5. It is of interest to note that the relative accuracy is greater for some high resonance frequencies than some low resonance frequencies. This is because of the mode shapes associated with the resonances at 307, 560, and 830 kHz. At 307 and 830 kHz, the maximum values of U and W in the cylinder occur at $r = a$, $z = L/2$. At 560 kHz, the maximum values of U on the curved surface and W in the cylinder occur at $r = a$, $z = L/2$. Modes with these characteristics are called surface modes, for example, by McMahon [26] who presented experimental values of the normalised frequency parameter $\omega a/c$, where $c = (Y/\rho)^{1/2}$. The frequency parameters for the resonances at 232.5 and 306.6 kHz are 1.4 and 1.9, respectively, and approximately the same as McMahon's results for $\sigma = 0.293$. It is seen from the expression for U_2 in Eq. (5c) that each term in the norm-wise set of functions that is complete in the axial direction is

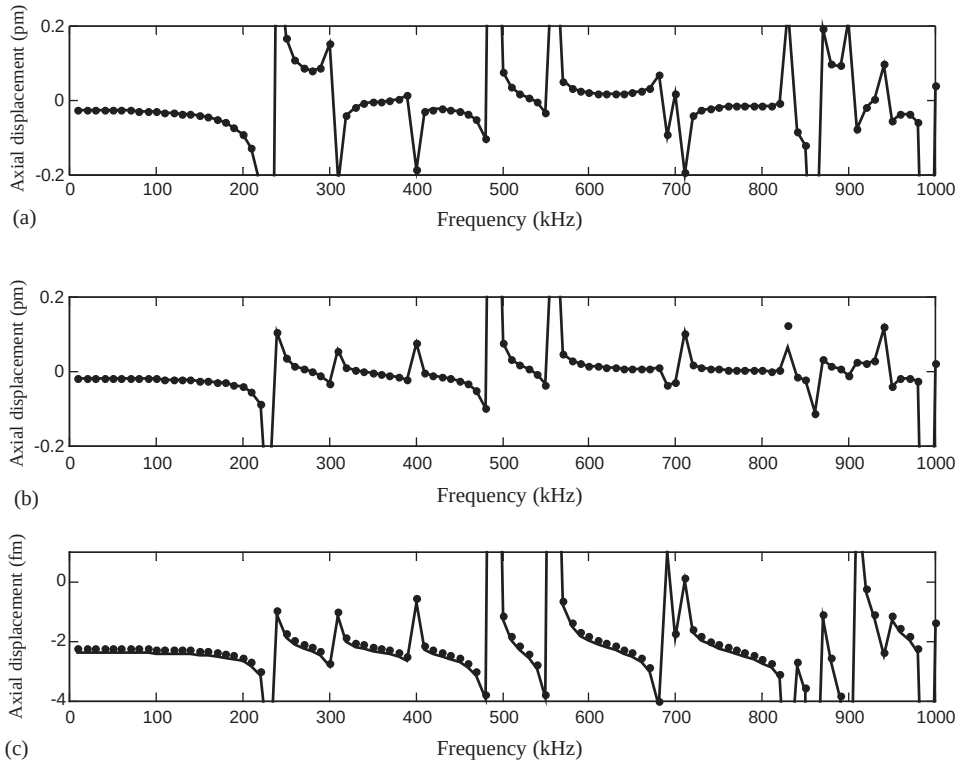

Fig. 2. Axial displacement, U, at $r = 0$, $z = L/2$ for Case 1A. Solid line: present method, dots: ATILA. (a) $N = 1$, (b) $N = 2$, and (c) $N = 20$.

zero at $z = L/2$. Further, it is seen from the expression for W_1 in Eq. (5b) that each term in the norm-wise set of functions that is complete in the radial direction is zero at $r = a$. Therefore, more terms in the series are required when the maxima in U and W occur at $r = a$, $z = L/2$.

The axial displacement, U, at $r = 0$, $z = L/2$ is shown in Figs. 2(a)–(c) for Case 1A, $N = 1$, 2, and 20, respectively. The agreement is good. The ATILA results in Figs. 2(a) and (b) are obtained by using 1600 square, equisized elements and those in Fig. 2(c) are obtained using a total of 2500 elements (400 square, equisized elements in the region $r \leqslant 0.1a$, $z \geqslant 0.95L$, 900 square, equisized elements in the region $r \geqslant 0.1a$, $z \leqslant 0.95L$ and 1200 rectangular, equisized elements elsewhere). For uniform stress, i.e., $N = 1$, at low frequencies, U on the flat surfaces is approximately equal to the static displacement $\bar{T}_{zz}L/(2Y) = 2.5 \times 10^{-14}$ m. The static result is obtained by using $T_{rr} = T_{\theta\theta} = T_{rz} = 0$ and $T_{zz} = \bar{T}_{zz}$ everywhere in the cylinder. All the resonances shown in Table 1 are seen in Fig. 2 also. In Fig. 2(b), at 830 kHz, the difference between the present method and ATILA is greater than at other frequencies. This occurs because there is a resonance at 830.5 kHz in ATILA and 830.8 kHz in the present method and the forced response is being compared at a frequency that is very close to the resonance frequency. This occurs in other figures also but is not obvious because some of the values are outside the displacement range shown in the figures.

Table 2
Axial displacement, U, at $r=0$, $z=L/2$ for Case 1A

Excitation N	Frequency (kHz)	Axial displacement, U (10^{-15} m)				
		ATILA [23]	Present method			
			$M_r=M_z=5$	$M_r=M_z=10$	$M_r=M_z=20$	$M_r=M_z=200$
1	100	−30.0	−30.1	−30.0	−30.0	−30.0
	200	−91.0	−91.3	−90.7	−90.9	−91.0
	300	154.4	148.2	149.6	152.9	154.3
	400	−184.3	−193.0	−185.3	−184.4	−184.3
	500	77.0	82.7	77.8	77.2	77.0
	600	21.6	21.8	21.9	21.7	21.6
	700	18.1	17.7	18.5	18.2	18.1
	800	−14.4	−15.4	−15.1	−14.6	−14.4
	900	220.4	210.8	216.9	219.5	220.5
	1000	41.2	41.9	41.4	41.2	41.2
2	200	−41.7	−40.8	−41.6	−41.5	−41.7
	500	76.0	83.0	76.7	76.2	76.0
	1000	20.7	21.4	20.5	20.7	20.7
20	200	−2.52	−1.07	−1.83	−2.66	−2.52
	500	−1.13	0.45	−0.40	−1.26	−1.12
	1000	−1.37	0.36	−0.63	−1.51	−1.37

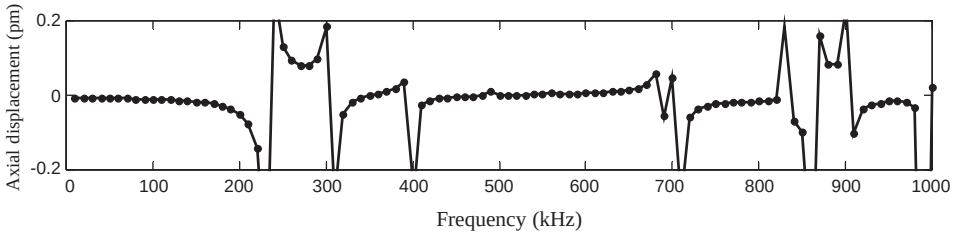

Fig. 3. Axial displacement, U, at $r=0$, $z=L/2$ for Case 1B, $N=2$. Solid line: present method, dots: ATILA.

The effect of the number of terms, M_r and M_z, in the series on the computed axial displacement, U, at $r=0, z=L/2$, is shown in Table 2 for Case 1A, $N=1$, 2, and 20 at 200, 500 and 1000 kHz. For $N=1$ and 2, it is seen that $M_r=M_z=10$ is sufficient get accuracies of interest in most practical cases. When N increases, the load is more concentrated and the number of terms required to obtain a similar relative accuracy also increases. Results are shown even for $M_r=M_z=200$ to indicate that the response can be determined to much more concentrated loads. It is seen from Eqs. (21) and (23) as well as from Table 2 that the values of M_r and M_z required to get reasonable accuracy depends primarily on the spatial distribution of the excitation and not on the frequency of excitation.

The axial displacement, U, at $r=0$, $z=L/2$ is shown in Fig. 3 for Case 1B, $N=2$. The agreement with the results obtained using ATILA is once again good. As expected, the sum of the responses

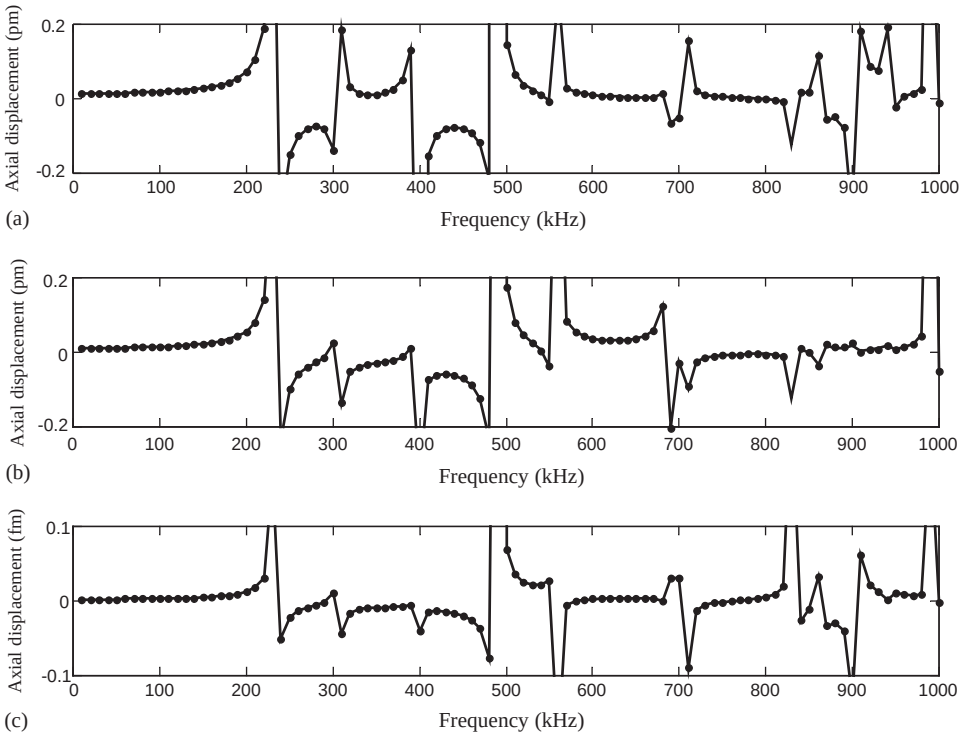

Fig. 4. Axial displacement, U, at $r = 0$, $z = L/2$ for Case 2A. Solid line: present method, dots: ATILA. (a) $N = 1$, (b) $N = 2$, and (c) $N = 20$.

to the excitations in Case 1A and 1B, $N=2$ is equal to the response to the excitation in Case 1A, $N=1$, i.e., the sum of the responses to excitations inside and outside a circle of radius $a/2$ is equal to the response to the excitation over a circle of radius a. It is seen by comparing Figs. 3 and 2(b) that the response at a particular frequency is strongly dependent on the spatial distribution of the excitation. For example, at 560 kHz, the responses in Fig. 2 are much greater than that in Fig. 3 indicating that the mode with a resonance frequency of 559 kHz is strongly excited by stresses acting at the centres of the flat surfaces.

The axial displacement, U, at $r=0$, $z=L/2$ is shown in Figs. 4(a)–(c) for Case 2A, $N=1$, 2, and 20, respectively Table 3 . The agreement with the results obtained using ATILA is good. For $N=20$, a total of 2500 elements and a fine mesh in the neighbourhood of $r=a$, $z=0$ are used. For $N=1$, at low frequencies, U is approximately equal to $\widetilde{T}_{rr}\lambda L/[2\mu(3\lambda+2\mu)] = \widetilde{T}_{rr}L\sigma/Y = 1.5\times10^{-14}$m. The static result is obtained by using $T_{rr} = T_{\theta\theta} = T_{rr}$ and $T_{zz} = T_{rz} = 0$ everywhere in the cylinder.

The axial displacement, U, at $r=0$, $z=L/2$ is shown in Fig. 5 for Case 2B, $N=2$. The agreement with the results obtained using ATILA is good. Again, the sum of the responses to the excitations in Case 2A and 2B, $N=2$ is equal to the response to the excitation in Case 2A, $N=1$. Again, all the resonances in Table 1 are seen in Figs. 4 and 5 though the magnitudes of the responses are dependent on the spatial distribution of stress.

Table 3
Axial displacement, U, at $r=0$, $z=L/2$ for Case 2A

Excitation N	Frequency (kHz)	Axial displacement, U (10^{-15} m)				
		ATILA [23]	Present method			
			$M_r=M_z=5$	$M_r=M_z=10$	$M_r=M_z=20$	$M_r=M_z=200$
1	100	19.4	19.4	19.3	19.4	19.4
	200	72.4	72.7	72.1	72.3	72.4
	300	−137.3	−132.0	−133.1	−136.0	−137.2
	400	−1147.5	−1201.7	−1154.1	−1148.7	−1147.5
	500	151.0	160.3	152.1	151.2	151.0
	600	10.2	10.3	10.3	10.2	10.2
	700	−48.7	−49.7	−49.7	−49.0	−48.7
	800	−0.52	−0.05	−0.17	−0.42	−0.52
	900	−310.4	−301.7	−308.0	−309.8	−310.5
	1000	−12.6	−18.4	−13.2	−12.6	−12.5
2	200	55.4	55.8	55.1	55.3	55.4
	500	180	192	182	181	180
	1000	−49.1	−52.3	−49.6	−49.1	−49.1
20	200	12.3	12.4	12.2	12.2	12.3
	500	68.9	72.0	69.3	69.0	68.9
	1000	−1.78	−3.34	−1.90	−1.79	−1.78

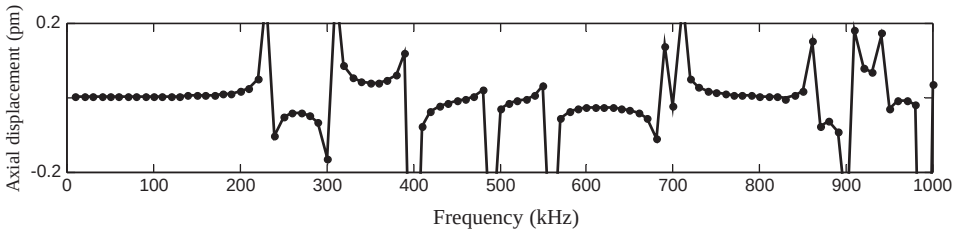

Fig. 5. Axial displacement, U, at $r=0$, $z=L/2$ for Case 2B, $N=2$. Solid line: present method, dots: ATILA.

5. Conclusions

A method is presented to determine the response of solid cylinders to axisymmetric distributed excitations. The method is based on the use of two infinite series solutions to the governing equations. Each term in the two series is an exact solution to the governing equations. The two series consist of terms that are orthogonal and form complete sets of functions in the axial and radial directions, respectively.

Numerical solutions are presented to illustrate free and forced vibration responses. It is seen that only a few terms of the infinite series are needed to compute a large number of resonance frequencies as well as determine the response to high-frequency loads on the flat and curved surfaces. The number of terms required depends primarily on the spatial distribution and not on the frequency of the excitation. For example, the response of a cylinder of length and diameter 10 mm each to uniform axial stress, acting inside a circle of radius 5 mm, on the flat surfaces is determined with an error of less than 1% even at 1 MHz using only 10 terms in each series. However, results obtained using 200 terms in each series are also presented to show that the response to very highly concentrated loads can be determined.

The method can be extended to determine the responses of solid and hollow cylinders to excitations that are not axisymmetric and neither symmetric nor antisymmetric about the centre of the cylinder. It can also be extended to analyse the response of piezoelectric cylinders to arbitrary excitations [27].

Acknowledgement

The authors thank the Director, Naval Physical and Oceanographic Laboratory, for granting permission to publish this paper.

References

[1] K.P. Soldatos, Review of three dimensional dynamic analyses of circular cylinders and cylindrical shells, *Applied Mechanics Reviews* 47 (10) (1994) 501–516.
[2] J.R. Hutchinson, Axisymmetric vibrations of a solid elastic cylinder encased in a rigid container, *Journal of the Acoustical Society of America* 42 (1967) 398–402.
[3] J.R. Hutchinson, Axisymmetric vibrations of a free finite length rod, *Journal of the Acoustical Society of America* 51 (1972) 233–240.
[4] J.R. Hutchinson, Vibrations of solid cylinders, *Journal of Applied Mechanics* 47 (1980) 901–907.
[5] J.R. Hutchinson, Vibrations of free hollow circular cylinders, *Journal of Applied Mechanics* 53 (1988) 641–646.
[6] C.P. Lusher, W.N. Hardy, Axisymmetric free vibrations of a transversely isotropic finite cylindrical rod, *Journal of Applied Mechanics* 55 (1988) 855–862.
[7] M. Rumermann, S. Raynor, Natural frequencies of finite circular cylinders in axially symmetric longitudinal vibration, *Journal of Sound and Vibration* 15 (1971) 529–543.
[8] G.M.L. Gladwell, U.C. Tahbildar, Finite element analysis of the axisymmetric vibrations of cylinders, *Journal of Sound and Vibration* 22 (1972) 143–157.
[9] G.W. McMahon, Finite-difference analysis of the vibration of solid cylinders, *Journal of the Acoustical Society of America* 48 (1970) 307–312.
[10] P.R. Heyliger, Axisymmetric free vibrations of finite anisotropic cylinders, *Journal of Sound and Vibration* 148 (1991) 507–520.
[11] K.P. Soldatos, V.P. Hadjigeorgiou, Three-dimensional solution of the free vibration problem of homogeneous isotropic cylindrical shells and panels, *Journal of Sound and Vibration* 137 (1990) 369–384.
[12] A.W. Leissa, J. So, Comparison of vibration frequencies for rods and beams from 1-D and 3-D analyses, *Journal of the Acoustical Society of America* 98 (4) (1995) 2122–2135.
[13] A.W. Leissa, J. So, Accurate vibration frequencies of circular cylinders from three-dimensional analysis, *Journal of the Acoustical Society of America* 98 (4) (1995) 2136–2141.

[14] J.R. Hutchinson, Comments on Comparison of vibration frequencies for rods and beams from one-dimensional and three-dimensional analysis [J. Acoust. Soc. Am. 98 (1995), 2136–2141], *Journal of the Acoustical Society of America* 100 (1996) 1890–1892;
A. Leissa, J. So, *Journal of the Acoustical Society of America* 100 (1996) 1893.
[15] J.R. Hutchinson, Comments on Accurate vibration frequencies of circular cylinders from three-dimensional analysis [J. Acoust. Soc. Am. 98 (1995), 2136–2141], *Journal of the Acoustical Society of America* 100 (1996) 1894–1895;
A. Leissa, J. So, *Journal of the Acoustical Society of America* 100 (1996) 1896.
[16] G.R. Buchanan, C.L. Chua, Frequencies and mode shapes for finite length cylinders, *Journal of Sound and Vibration* 246 (5) (2001) 927–941.
[17] L. Kari, Axially symmetric modes in finite cylinders—the wave guide solution, *Wave Motion* 36 (2002) 169–184.
[18] L. Kari, Erratum to "Axially symmetric modes in finite cylinders—the wave guide solution [Wave Motion 36 (2002), 169–184]", *Wave Motion* 37 (2003) 191–206.
[19] D. Zhou, Y.K. Cheung, S.H. Lo, F.T.K. Au, 3D vibration analysis of solid and hollow circular cylinders via Chebyshev-Ritz method, *Computer Methods in Applied Mechanical Engineering* 192 (2003) 1575–1589.
[20] R. Holland, E.P. Eer Nisse, *Design of Resonant Piezoelectric Devices*, Research Monograph No. 56, MIT Press, Cambridge, MA, 1969.
[21] K.T. Chau, X.X. Wei, Finite solid circular cylinders subjected to arbitrary surface load. Part I—Analytic solution, *International Journal of Solids and Structures* 37 (40) (2000) 5707–5732.
[22] X.X. Wei, K.T. Chau, Finite solid circular cylinders subjected to arbitrary surface load. Part II—Application to double-punch test, *International Journal of Solids and Structures* 37 (40) (2000) 5733–5744.
[23] J.N. Decarpigny, J.C. Debus, B. Tocquet, D. Boucher, In-air analysis of piezoelectric tonpilz transducers in a wide frequency band using a mixed finite element-plane wave method, *Journal of the Acoustical Society of America* 78 (1985) 1499–1507 ATILA is developed by Acoustic Laboratory, I.S.E.N., Lille, France.
[24] H. Kolsky, *Stress Waves in Solids*, Dover Publications, New York, 1953 1963 re-issue.
[25] M. Abramowitz, I.A. Stegun (Eds.), *Handbook of Mathematical Functions*, Dover Publications, New York, 1965 Eqs. 11.3.20, 11.3.29, and 11.4.5.
[26] G.W. McMahon, Experimental study of the vibrations of solid, isotropic, elastic cylinders, *Journal of the Acoustical Society of America* 36 (1) (1964) 85–92.
[27] D.D. Ebenezer, R. Ramesh, Analysis of axially polarized piezoelectric cylinders with arbitrary boundary conditions on flat surfaces, *Journal of the Acoustical Society of America* 113 (4) (2003) 1900–1908.